Nanoscale

PAPER

View Article Online
View Journal | View Issue

Cite this: *Nanoscale*, 2023, **15**, 2891

Langmuir and Langmuir–Blodgett technologies as nanoarchitectonic tools for the incorporation of curcumin in membrane systems†

Laura Dotor, [a,b,c] José Miguel García-Pinilla, [a,b,c] Santiago Martín [a,b,c] and Pilar Cea *[a,b,c]

Curcumin (CCM) is a molecule of particular interest in health applications due to its wide spectrum of benefits for humans. However, its water-insoluble character and low bioavailability have so far prevented its extended use as a therapeutic agent. Incorporation of CCM in drug delivery vehicles (liposomes, vesicles, exosomes, *etc.*) is expected to contribute to increasing its bioavailability. Studies of the affinity of CCM with the components of the membrane systems of such vehicles and determination of factors that may enhance curcumin entrapment in biological membranes are of fundamental importance. To that end, here we take advantage of the nanoarchitectonic capabilities of the Langmuir technique for the construction of model cell membranes and determination of thermodynamic properties in mixed films. The obtained results may serve to: (i) provide some light on the miscibility of CCM with the components in the cell membrane and (ii) determine the optimal conditions for the fabrication of membrane systems incorporating CCM. For that, binary and ternary mixed Langmuir films of CCM, DPPC (1,2-dipalmitoyl-*sn*-*glycero*-3-phosphocholine) and CHOL (cholesterol) have been prepared. Whilst binary mixtures of DPPC and CCM exhibit poor miscibility and even phase segregation, CHOL has shown itself as a key element to promote the incorporation of CCM in the phospholipidic membrane containing DPPC. Both the thermodynamic studies of the ternary Langmuir films and the Atomic Force Microscopy (AFM) images of Langmuir–Blodgett films have shown that ternary mixed films with a molar fraction composition of $x_{DPPC}/x_{CHOL}/x_{CCM}$ = 0.4/0.4/0.2 exhibit good miscibility, stability, and result in monolayers with a very homogeneous topography.

Received 27th November 2022,
Accepted 3rd January 2023

DOI: 10.1039/d2nr06631a

rsc.li/nanoscale

Introduction

Curcumin is the major compound (77%) of turmeric (Curcuma longa), which is a flowering plant of the Zingiberaceae (ginger) family that grows in the tropics and subtropics of Asia, especially in countries such as India, China, Pakistan, Thailand and Indonesia,[1] as well as in Australia, the South Pacific and tropical regions.[2] From a historical perspective, turmeric was named for the first time in the book Xinxiu bencao, published in 659 A.D. and considered as the "first pharmacopoeia in the world".[3] The curcumin compound was isolated from turmeric for the first time in 1815 and identified as diferuloylmethane in 1910;[4] its chemical tautomeric structure (keto and enol isomers) is shown in Fig. 1. Curcumin has been widely employed for more than four millennia as a traditional medicine, natural dye and food condiment in the abovementioned regions. Additionally, it is the main ingredient of curry, whose use was extended in Europe by the United Kingdom and the Netherlands, transferring the knowledge acquired in their colonies during the 18th century. Currently, curcumin is commonly used worldwide as food coloring, flavoring agent and additive.[5] Thus, curcumin is an authorized colorant in the European Union under the E100 code; curcuminoids have also been recognized in 2020 as "GRAS" (acronym for Generally Recognized as Safe) by the FDA (Food and Drug Administration in the United States). In addition, curcumin is scientifically considered as a relevant compound that deserves further investigation[6] for its potential use in pharmaceutical applications due to its numerous beneficial effects for humans. These include anti-carcinogenic, antioxidant, antimicrobial, antiviral, antidepressant, anti-rheumatic, hepato- and nephron-protective, hypoglyceric character, thrombosis suppressing, myocardial infarction protective, as

[a]*Instituto de Nanociencia y Materiales de Aragón (INMA), CSIC-Universidad de Zaragoza, 50009 Zaragoza, Spain. E-mail: pilarcea@unizar.es*
[b]*Laboratorio de Microscopias Avanzadas (LMA), Universidad de Zaragoza, 50018, Zaragoza, Spain*
[c]*Departamento de Química Física, Facultad de Ciencias, Universidad de Zaragoza, 50009 Zaragoza, Spain*

† Electronic supplementary information (ESI) available. See DOI: https://doi.org/10.1039/d2nr06631a

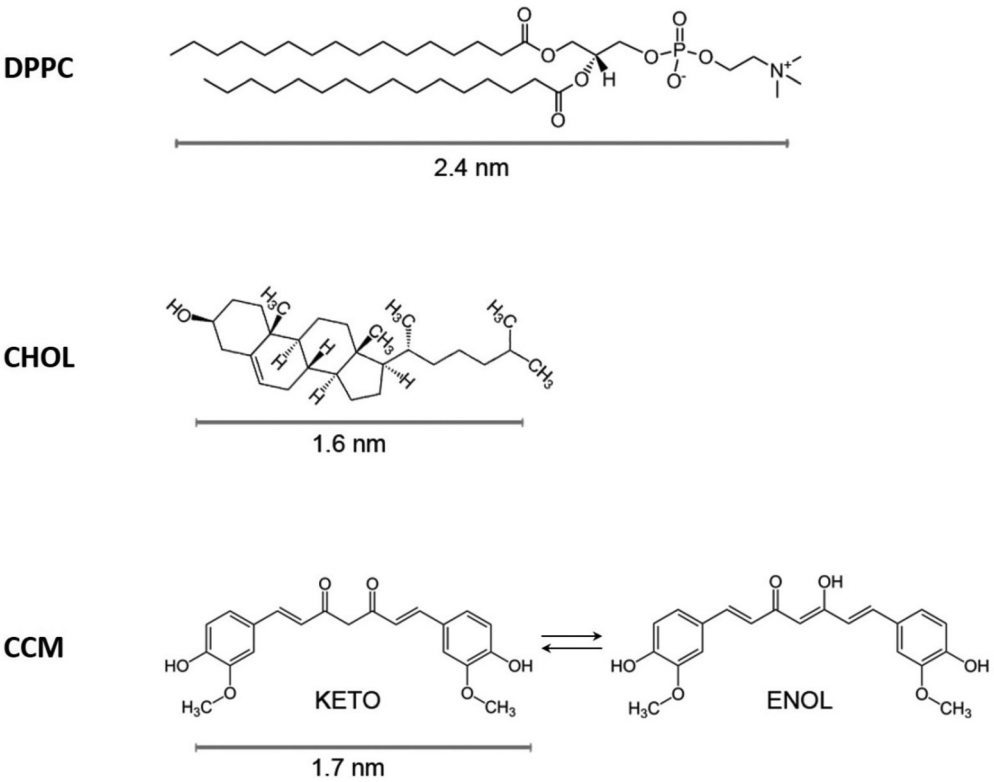

Fig. 1 Chemical structure of the materials used in this contribution: DPPC (dipalmitoylphosphatidylcholine), CHOL (cholesterol) and CCM (curcumin).

well as immunomodulatory and anti-inflammatory capabilities. All these recognized properties of curcumin have been documented in a vast amount of research, which has been gathered in comprehensive reviews.[1,7–19] Importantly, clinical studies in humans have proven that curcumin is generally safe even at high daily doses of up to 12 grams with only a few minor side-effects,[20] and more recently it has been reported that oral ingestion of curcumin is not toxic to humans up to 8 g per day for 3 months.[21] All these evidences have oriented investigators and the general public to view curcumin as a panacea, albeit not exempt of controversial opinions,[6,22,23] and the construction of intended puns such as "curecumin"[24] or sensational titles in scientific papers such as "From kitchen to clinic", "From farm to pharmacy", "Curry against Alzheimer", "the Indian solid gold", "Golden spice", "A future nanomedicine for cancer", "an age-old spice with modern targets", "too good to be true?", "Spicing up of the immune system by curcumin", *etc*.

Despite the potential applicability of curcumin and its recognition as a pharmacodynamically fierce molecule capable of hitting many targets at a time, no form of curcumin nor closely related analogue compound seems to possess two of the most relevant properties required for a good drug candidate, namely high water solubility and high bioavailability, which hampers its use as a therapeutic agent. Researchers are trying to circumvent bioavailability problems of curcumin (low serum levels, limited tissue distribution, poor absorption, apparent rapid metabolism and short half-life) with the use of adjuvants or absorption factors (piperidine/piperine), phospholipid complexes, metal-curcumin complexes, or its encapsulation into cyclodextrins, nanoparticles, liposomes, micelles, dendrimers, gels, DNA-nanostructures, or even exosomes.[19,25–35] Enhanced bioavailability of curcumin in the near future by these media is likely to bring this promising natural product to the forefront of therapeutic agents for treatment of human diseases. Before this occurs, additional studies are required both at a fundamental and preclinical state. Thus, the interactions of curcumin with biological cell membranes should be further studied for a better understanding of curcumin penetration/retention by the membrane.[29,36] Also, studies of the affinity of curcumin with membrane systems (micelles, liposomes, exosomes) and elucidation of factors that may influence curcumin entrapment efficiency might contribute to the design of new strategies for the construction of optimized drug delivery vehicles.

Because of the high complexity of *in vivo* studies using biological membranes,[37] model cell membranes are often employed for fundamental research.[38–42] The Langmuir technique is a widely used method for the controlled arrangement of nano-sized structural units in an intended configuration (nanoarchitectonics), in this case, the construction of model cell membranes; it also permits the systematic study of interactions between the components in the cell membrane as well as the interaction of such natural components with xeno-

biotics, drugs, nanoparticles, *etc*.[43–47] However, and to the best of our knowledge, a rather limited number of contributions have been published involving Langmuir and Langmuir–Blodgett techniques for the incorporation of curcumin (henceforth abbreviated as CCM) into model cell membranes. These contributions were focused on the study of a few molar fractions of CCM-DPPC (1,2-dipalmitoyl-*sn-glycero*-3-phosphocholine) binary systems,[48] and mixtures of CMM and cetyl palmitate (acting as a solubilizing agent of CCM) added to DOPC (1,2-dioleoyl-*sn-glycero*-3-phosphatidylcholine).[49] For these reasons, in this contribution we extend this previous work in the literature to the study of mixed Langmuir films incorporating DPPC (1,2-dipalmitoyl-*sn-glycero*-3-phosphocholine), CHOL (cholesterol: 10,13-dimethyl-17-(6-methylheptan-2-yl)-2,3,4,7,8,9,11,12,14,15,16,17-dodecahydro-1*H*-cyclopenta[*a*]phenanthren-3-ol) and CCM (1,7-bis-(4-hydroxy-3-methoxyphenyl)-1,6-heptadiene-3,5-dion), with their chemical structures illustrated in Fig. 1. In particular, binary and ternary mixed Langmuir films have been prepared, and the obtained surface pressure *vs.* area per molecule isotherms have been subjected to a comprehensive thermodynamic analysis of the properties exhibited by these mixtures. The simplified model cell membrane here used (incorporating DPPC and CHOL) was chosen for a number of reasons: (i) phospholipids incorporating choline as a headgroup (*i.e.* phosphatidylcholines, PC) – as in DPPC – are the most abundant ones in mammalian cell membranes;[50] (ii) in particular, DPPC is the major component in the membranes of lung cells (pulmonary alveolus to be more specific with DPPC preventing alveolar collapse during breathing by reducing the surface tension of the water layer where gas exchange occurs);[51] in addition, it presents neutral charge and high stability;[52] (iii) CHOL is a key compound in cell membranes that modulates the fluidity and the asymmetry of the bilayer;[53] (iv) eukaryotic plasma membranes contain up to one molecule of cholesterol for every phospholipid molecule[50] (this is the reason why we will make emphasis later in the paper in the DPPC/CHOL x_{DPPC}/x_{CHOL} = 0.5/0.5 proportion); (v) phospholipids and sterols (including DPPC and CHOL) are also the major elements used in liposomal preparations,[52] *i.e.*, a major understanding of curcumin miscibility and stability in a biomimetic membrane would contribute to improve formulations in liposomes incorporating CCM as a co-adjuvant of other cargo drugs. As we will see below, whilst DPPC and CCM exhibit phase separation and a poor miscibility, CHOL plays a relevant role as a solubilizing agent, with DPPC/CHOL/CCM mixtures in the $x_{DPPC}/x_{CHOL}/x_{CCM}$ = 0.4/0.4/0.2 proportion resulting in stable Langmuir monolayers and homogeneous Langmuir–Blodgett films.

The main novelties of this contribution rely on (i) the demonstration that the interactions of CHOL with curcumin are crucial in the case of ternary mixtures to obtain homogenous and well-mixed films incorporating DPPC/CHOL/CCM and (ii) the applicability of these thermodynamic studies at the air–water interface as a useful tool to determine the optimal composition in model cell membranes, which may be relevant in liposomal formulations.

Materials and methods

Materials

Appropriate amounts of curcumin (CCM, ≥99%, Sigma-Aldrich), cholesterol (CHOL, ≥99%, Sigma-Aldrich) and dipalmitoylphosphatidylcholine (DPPC ≥99%, Sigma-Aldrich) were dissolved in chloroform to prepare stock solutions of 0.01 μmol mL^{-1}, 0.1 μmol mL^{-1} and 0.1 μmol mL^{-1}, respectively. The concentration of CCM either pure or in the mixtures was as low as 10^{-5} M to prevent the formation of three dimensional aggregates; these experimental conditions resulted in reproducible isotherms. Chloroform was purchased from Macron Fine Chemicals (≥99.8%). The binary (CCM/DPPC, CCM/CHOL and DPPC/CHOL) and ternary systems (CCM/DPPC/CHOL) were prepared by mixing the proper volumes of the stock solutions to obtain the target molar fractions of the components in the mixture.

Methods

Langmuir technique. Surface pressure *vs.* area per molecule (π-A) isotherms were recorded on a pure water sub-phase (Millipore Milli-Q purification system, resistivity 18.2 MΩ cm) using a KSV Nima KN 2003 Teflon trough (580 × 145 mm^2). The surface pressure (π) of the monolayers was determined using a Wilhelmy paper plate pressure sensor. All the experimental setup was contained in a constant temperature (20 ± 1 °C) semi-clean room. A constant initial area per molecule (1.30 nm^2) was used for all the experiments: the appropriate volume of the solutions was spread on the water surface by using micro-syringes (Hamilton–Bonaduz from Sigma Aldrich). The solvent was allowed to evaporate 15 minutes before starting the compression of the monolayer, with the trough barriers moving at a constant rate of 10 mm min^{-1}. All isotherms were recorded at least three times to confirm their reproducibility.

Transfer of Langmuir films to form Langmuir–Blodgett (LB) films. Using the same experimental setup as before, selected monolayers were transferred onto mica substrates to form one-monolayer LB films by the withdrawal of a substrate initially immersed in the water subphase. These LB films were subsequently characterized by Atomic Force Microscopy. Mica sheets were provided by Electron Microscopy Sciences Company (Cat. #71851-05, sheet size 1″ × 3″; 25 × 75 mm and thickness 0.26–0.31 mm). Each mica substrate was cut by using scissors into *ca.* 1 × 1 cm^2 pieces, which were cleaved with adhesive tape prior to their use. The monolayers at the air–water interface were transferred at a constant surface pressure by the vertical dipping method (emersion). The dipping speed was 2 mm min^{-1}. The chosen surface pressure of transference (30 mN m^{-1}) mimics the lateral pressure in biological membranes.

Atomic force microscopy (AFM). Topographic images of the LB films were obtained by means of a Multimode 8 microscope equipped with a Nanoscope V control unit from Bruker at a scan rate of 1.0–1.2 Hz, using Tapping mode. The data were collected using RTESPA-150 tips (nominal frequency of 150

kHz, from Bruker) in air. The images were processed by using Gwyddion Software. Differences in height between monolayer domains were determined by performing section analysis and areas percentages in segregated domains using a mask by threshold and subsequent bearing analysis.

Results and discussion

The Langmuir technique is a widely used method for preparing model cell membranes.[47] By using this methodology, intermolecular interactions between the membrane components as well as between the membrane components and drugs, xenobiotics, nanoparticles, *etc*. can be determined together with their influence on the molecular alignment. Here, the chosen model cell membrane contains a phospholipid, namely dipalmitoylphosphatidylcholine, DPPC, and cholesterol, CHOL, Fig. 1. The use of this simplified model cell membrane is expected to provide information on (i) the miscibility of curcumin, CCM, with the lipids (DPPC and CHOL) in the cell membrane; (ii) the stability of the membrane incorporating CCM and (iii) the composition of the most stable ternary mixed monolayers at 30 mN m^{-1} in which the DPPC/CHOL proportion is x_{DPPC}/x_{CHOL} = 0.5/0.5. We pay particular attention to this surface pressure, 30 mN m^{-1}, because, on the one hand, it is estimated to be the biological surface pressure[54,55] and, on the other hand, the transference of x_{DPPC}/x_{CHOL} = 0.5/0.5 mixed monolayers at this surface pressure is well reported in the literature.[42,56] DPPC/CHOL x_{DPPC}/x_{CHOL} = 0.5/0.5 LB films are highly homogeneous, which may help to discern any change in the ternary mixtures induced by the presence of CCM. Additionally, as indicated above, the eukaryotic plasma membranes contain up to one molecule of cholesterol for every phospholipid molecule.[57] For these reasons, the thermodynamic behaviour of Langmuir mixed films integrated by (DPPC/CHOL), (DPPC/CCM) and (CHOL/CCM) in the whole range of molar fractions and surface pressures has been investigated followed by a comprehensive study of the ternary mixtures (DPPC/CHOL/CCM) and the subsequent AFM analysis of the LB films.

Fig. 2 shows the surface pressure–area per molecule (π–A) isotherms and the compression modulus–surface pressure (K_s–π) plots for the monolayers of the three pure compounds here studied, namely DPPC, CHOL and CCM. The compression modulus values (inverse of the compressibility, C_s), $K_s = C_s^{-1}$, were calculated directly from the π-A isotherm data using eqn (1):[35]

$$K_s = C_s^{-1} = -A\left(\frac{d\pi}{dA}\right)_{p,T} \quad (1)$$

The compression modulus is of paramount importance since it provides information about the physical state of monolayers, and it is strictly associated with the packing and ordering of molecules at the air–water interface. The different phases and phase transitions in the π-A isotherms can be determined based on the Davies and Rideal classification.[58] The liquid-expanded (LE) phase is characterized by compression modulus values between 12.5 and 50 mN m^{-1}, while the liquid condensed (LC) phase shows K_s values between 100 and 250 mN m^{-1}. Finally, the solid phase (*S*) shows K_s values above 1000 mN m^{-1}.

Single monolayers

Since DPPC and CHOL monolayers and their mixtures have been widely reported in the literature,[38,52,56,59–66] here we focus on the discussion of CCM monolayers; albeit a summary of the most relevant results for both DPPC and CHOL single and mixed monolayers is included in the ESI (Fig. S1 and S4–S7†).

CCM has a large tendency for aggregation and according to our results the isotherms are only fully reproducible when the spreading solution has a concentration around 10^{-5} M, plus sonication for 2 min before spreading, to prevent molecular aggregation (which considering our trough dimensions results in a spreading volume of 10 mL; such a volume was slowly spread to permit the solvent evaporation and prevent surface saturation; the spreading time was *ca.* 1 hour). For this reason, the isotherms here presented were recorded under this premise. Additionally, the mixed films were prepared employing a constant initial area per molecule of 1.30 nm^2 for the mixed (binary and ternary) films. The reproducible CCM isotherm here presented exhibits a lift-off at *ca.* 0.23 nm^2 per molecule. K_s reaches a maximum of 83 mN m^{-1}, *i.e.*, the monolayer remains in a liquid-expanded phase till the collapse of the monolayer occurs at 51 mN m^{-1}. The surface behaviour of CCM is tentatively interpreted here in terms of the chemical structure of CCM, which is a symmetric molecule, with -OH groups in opposite ends of the molecule. CCM is a α–β unsaturated diketone (Fig. 1), so it exhibits keto–enol tautomerism[67] (the enolic form predominates both in aqueous and organic solvents). Therefore, the high number of hydrogen bond acceptors and donors leads to an extensive dynamic intermolecular hydrogen bond network and possibly also to the formation of hydrogen bonds with water molecules on the surface. In addition, the presence of the p-phenolic rings, may result in intermolecular π–π stacking. On the other hand, CCM contains a high number of rotatable bonds and lack of long alkyl chains. All these factors together promote a high conformational flexibility, and dynamic hydrogen bonding structures that contribute to the fluidity of the monolayer. The number of π-A isotherms reported in the literature for CCM is rather limited.[48,49,68] For instance, Karewicz *et al.*[68] reported pure and mixed isotherms of CCM with lipid monolayers (EYPC, *i.e.* phosphatidylcholine from egg yolk). The isotherm for CCM only reached a surface pressure of *ca.* 10 mN m^{-1} with K_s values in the same order to the ones presented here in that range of surface pressures. The spreading concentration is not reported in that contribution, which is a crucial parameter according to our observations. Additionally, Xu *et al.*[48] reported CCM isotherms that reached a surface pressure higher than 50 mN m^{-1}, with a profile comparable to those shown here and also with K_s values in the same order of magnitude to the reported here. Xu *et al.*[48] used a higher concen-

tration for the spreading solution (*ca.* 2.7×10^{-4} M) than the one employed here and also a mixture of $CHCl_3$: methanol 3 : 1 not required in this work due to the lower concentration of CCM in $CHCl_3$ where it is fully miscible. Methanol could have an influence on the hydrogen bonds between CCM molecules and its solubility in water could result in partial penetration on the subphase and for these reasons it was not introduced in this work. These different experimental conditions (also including different temperature and compression speed) may explain that the CCM isotherms are not identical, although they are comparable. However, among all the different experimental conditions between this work and previous contributions,[48,49,68] the use of a very diluted solution of CCM plus sonication is the key parameter since according to our observations, at higher concentrations of CCM (>2×10^{-5} M) non-reproducible isotherms are obtained.

The stability of the CCM monolayers at the air–water interfase was evaluated in this contribution by recording the percentage loss of the area per molecule at a constant surface pressure of 30 mN m^{-1} (see Fig. S2 in the ESI†). A 15% loss in the first hour after the target surface pressure was attained, indicative of a certain instability which is consistent with the fluidity of the monolayer at this surface pressure (Fig. 2). Additionally, compression and decompression cycles for the CCM monolayers at the air–water interface were recorded. The π-A isotherm for the first cycle exhibits a negligible hysteresis (Fig. S3†). In the second compression cycle, the π-A isotherms followed almost the same trajectory as in the first compression with only a slight displace towards lower molecular areas followed again by a negligible hysteresis. These results indicate that no significant loss of molecules towards the subphase occurs upon the compression process.

Binary systems

The isotherms for the three binary mixtures here studied are shown in Fig. S1† (DPPC/CHOL) and Fig. S4† (DPPC/CCM and CHOL/CCM). The collapse surface pressure, π_{col}, of the mixed monolayers can be employed to elucidate between miscibility and immiscibility of the components according to the Crisp rule.[69] If the components are ideally miscible, the collapse will occur at intermediate pressures between the π_{col} of the pure components, being proportional to the molar fraction of the components in the mixture, whereas if the components are totally immiscible, the collapse will occur at the π_{col} of the component with the lowest π_{col}. In systems containing CCM, deviations from ideality in the π_{col} of the mixtures are observed, which is indicative of partial miscibility between the components (see the detailed π_{col} values *vs.* composition for the two binary systems containing CCM in Fig. S5†). In addition, the characteristic plateau in the DPPC single monolayer (Fig. 2) turns into a slope change in the mixed films (Fig. S4†). Also, the phase transitions occur at higher surface pressures for the binary mixtures incorporating CCM than for the DPPC or CHOL single monolayers (Fig. S4†). The reason of these observations is the clear tendency of the CCM to decrease the K_s values at a given surface pressure in both the (DPPC/CCM) and (CHOL/CCM) mixed monolayers, *i.e.* the monolayers become more compressible (more fluid) under the presence of CCM (Fig. S4†). Additionally, the K_s maximum values have also been determined for the isotherms (Fig. S5†). This is another parameter accounting for the miscibility and, importantly, the fluidity of the mixed films, with CCM decreasing the ideal K_s maximum value in DPPC and specially in the CHOL binary mixtures.

Another criterion to evaluate the miscibility and molecular interactions (attractive or repulsive) between the components in the monolayer is the thermodynamic excess area of mixing, A^E, defined as:[70]

$$A^E = A_{mix} - A_{ideal} = A_{mix} - \sum_i x_i A_i \quad (2)$$

where A_{mix} is the molecular area of the experimental mixed monolayer at the chosen surface pressure, π; A_i is the molecular area of the pure components at the surface pressure π

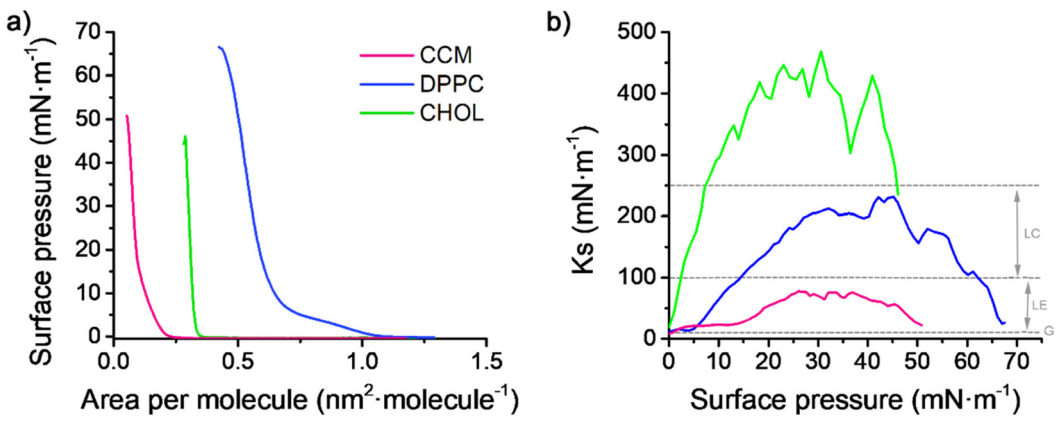

Fig. 2 (a) π-A isotherms for the monolayers of CCM, DPPC and CHOL at 20 °C. (b) K_s–π plots for the monolayers of CCM, DPPC and CHOL as obtained from the isotherms in (a). The lines and arrows in grey are indicative of the different phases of the monolayer according to the classification of Davies and Rideal.[58]

and x_i is the molar fraction. Excess areas inform about not only molecular interactions but also packing of the molecules in the mixed films (intermolecular accommodation and or dehydration interactions between the components in the mixed film).[71] When $A^E = 0$, the components of the monolayer are ideally miscible or totally immiscible, meanwhile if $A^E \neq 0$ the components are partially miscible. Negative deviations generally indicate attractive interactions between the components and/or a more effective packing of the molecules in the mixed films (or even formation of complexes between the components with the subsequent associated steric effects[72]), while positive deviations are indicative of repulsive interactions and/or a less efficient packing of the molecules in the mixed film. The excess area values for the three binary systems (Fig. S7†) exhibit small negative deviations from ideality at high surface pressures (30–40 mN m^{-1}). However, the (DPPC/CCM) excess areas at low surface pressures show positive deviations, indicating either repulsive interactions between these two components or rupture of DPPC-DPPC and/or CCM-CCM interactions. Xu *et al.*,[48] in contrast with our results, showed negative deviations in the (DPPC/CCM) excess areas for the whole range of molar fractions. We interpret such a difference in terms of the different experimental conditions (concentration of the spreading solution, presence of methanol as a co-spreading solvent by Xu *et al.*, different temperature and compression speed), which may result in a different behaviour of the mixed films at the air–water interface. As mentioned before, the concentration of the spreading solution is the most important parameter, which may have a significant impact on the overall interactions in the mixed layers and thereby could result in a different sign in the excess areas.

Additionally, the mixture of the components is also associated with the energy of the mixing process and also to the loss of entropy upon compression as well as to the energy related to phase transitions.[73] At constant p and T, the Gibbs surface excess energy of mixing, ΔG_m^E, is defined as:[74,75]

$$\Delta G_m^E = \int_0^\pi A_{mix} d\pi - \sum_i x_i \int_0^\pi A_i d\pi \quad (3)$$

Negative values of ΔG_m^E indicate strong interactions between the components, while positive values reveal weaker or even repulsive interactions between the components in the mixed film in comparison with the pure compounds. The Gibbs energy of mixing, ΔG_m, provides further information of the interactions between the monolayer components and stability of mixed films. Taking into account that:[76]

$$\Delta G_m^{ideal} = RT \sum_i x_i \ln x_i \quad (4)$$

the Gibbs energy of mixing can be calculated as:[76]

$$\Delta G_m = \Delta G_m^E + \Delta G_m^{ideal} \quad (5)$$

The increase in ΔG_m values for the (DPPC/CCM) mixtures as the surface pressure increases reaching positive ΔG_m values (Fig. S7†) at high surface pressures together with the presence of two minima in the ΔG_m *vs.* x_{DPPC} graph is indicative of unstable films exhibiting a poor miscibility between the components and phase segregation.[49,72,77] This result is in good agreement with previous contributions indicating that the insertion of CCM in lipid bilayers is a high energetic process.[78] CCM is a highly conjugated structure which may weaken hydrophobic interactions among alkyl chains in DPPC. In contrast, the (CHOL/CCM) mixtures exhibit negative ΔG_m values for the whole range of molar ratios (minimum at $x_{CCM} = 0.6$ and 0.8). These results are indicative of stable (CHOL/CCM) monolayers.

In conclusion, the above results indicate that the three binary mixtures (DDPC/CHOL), (DPPC/CCM) and (CHOL/CCM), exhibit a partial miscibility in the mixed Langmuir monolayers. CCM induces a fluidization of the mixed (DPPC/CCM) with the emergence of repulsive forces between the two molecules and phase segregation. Importantly, the (CHOL/CCM) binary mixture results in stable monolayers exhibiting attractive interactions between the components. This result suggests that CHOL may serve as a material of interest in membrane systems for the incorporation of CCM in the phospholipid matrix. Therefore, we will now consider the ternary mixtures of the three components to confirm this hypothesis.

Ternary system

A detailed study of (CCM/DPPC/CHOL) ternary systems was performed by recording the surface-pressure *vs.* area per molecule. In particular, 70 mixtures with different molar ratios of these components (Fig. S8†) were studied. The isotherms corresponding to the monolayers of these 70 mixtures were recorded (Fig. S9†) and from them, A^E (Fig. 3), K_s (Fig. 4), ΔG_m^E (Fig. S10†) and ΔG^E (Fig. 5) were determined at different surface pressures.

At surface pressures up to 15 mN m^{-1} the addition of CCM to the (DPPC/CHOL) mixture in the low CHOL ratio region results in positive excess areas (green areas in Fig. 3), *i.e.* the addition of CCM results in an increase of the area per molecule with respect to the ideal one, which is indicative of repulsive interactions between the components, that is, the addition of CCM possibly breaks DPPC-DPPC and DPPC-CHOL interactions. These repulsive interactions reach their maximum at $x_{DPPC}/x_{CHOL}/x_{CCM}$ = 0.05/0.05/0.9 (A^E = 0.43 nm^2 per molecule at 5 mN m^{-1}). As the surface pressure increases the excess area values decrease, with mixed monolayers showing negligible deviations from the additivity rule at surface pressures higher than 30 mN m^{-1} (dark blue areas) and even slightly negative deviations at 40 mN m^{-1} (purple areas). The addition of CCM to the (DPPC/CHOL) mixtures for larger CHOL ratios exhibits a similar trend although the excess area values are lower for the whole range of surface pressures. The minimum excess area value (A^E = −0.04 nm^2·per molecule) is obtained for $x_{DPPC}/x_{CHOL}/x_{CCM}$ = 0.4/0.2/0.4 and for $x_{DPPC}/x_{CHOL}/x_{CCM}$ = 0.1/0.2/0.7 at 40 mN m^{-1}. This observation, A^E decreasing with increasing surface pressure, is indicative of less repulsive interactions between the components as the monolayers are compressed.

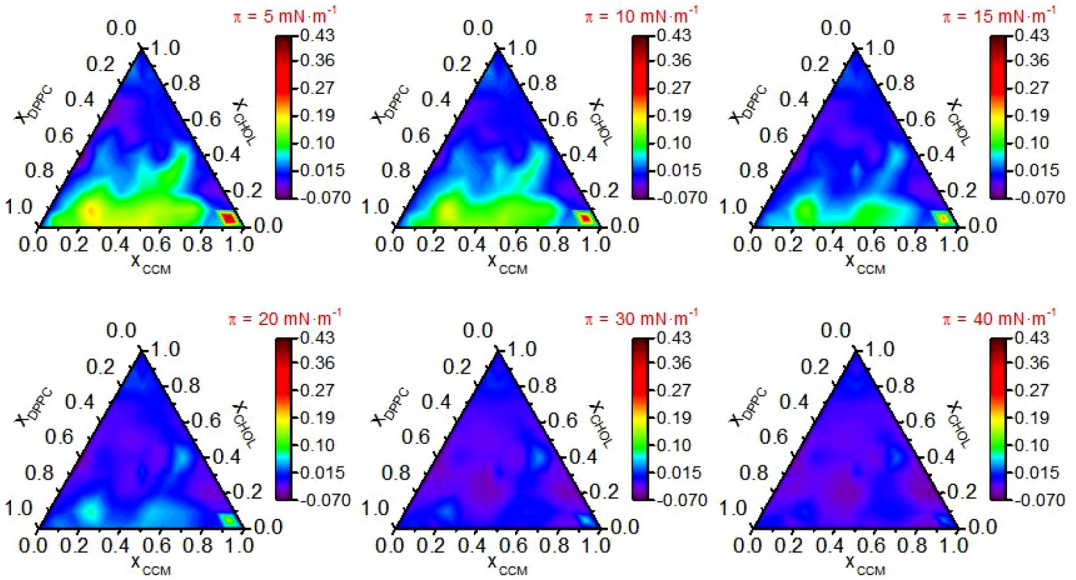

Fig. 3 Excess molecular area, A^E, in nm^2 per molecule *vs.* molar fraction in (DPPC/CHOL/CCM) ternary systems for the indicated surface pressures.

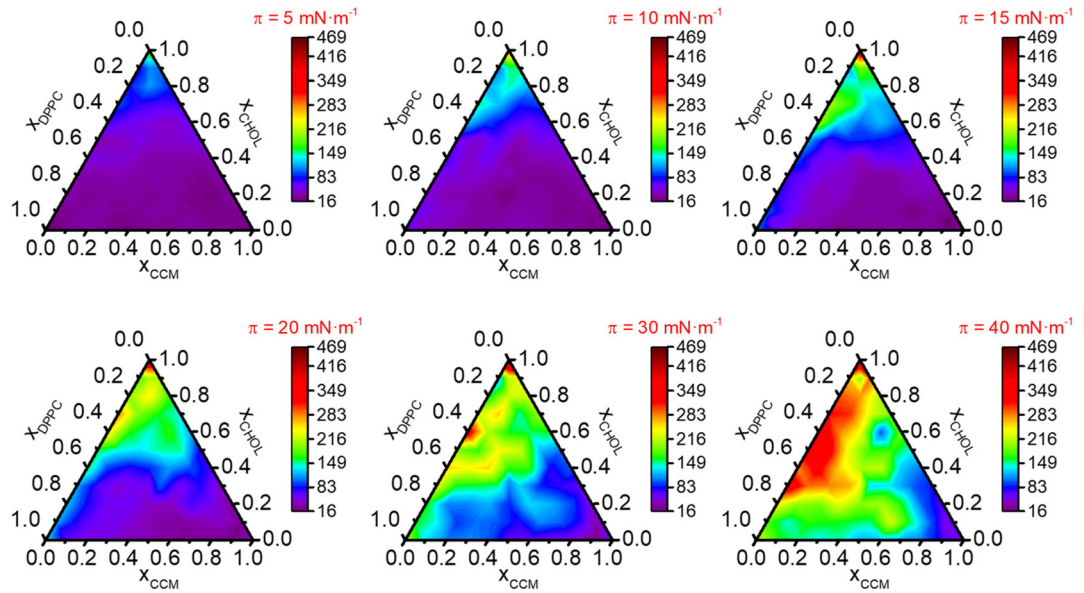

Fig. 4 K_s expressed in mN m^{-1} *vs.* molar fraction in (DPPC/CHOL/CCM) ternary system for the indicated surface pressures.

Fig. 4 shows K_s values *versus* film composition. At low surface pressures (5–15 mN m^{-1}) the ternary mixed films having $x_{CHOL} < 0.5$ and $x_{DPPC} > 0.5$ (purple regions) are in a LE phase; as the molar fraction of CHOL increases, a LE-LC transition phase (dark blue regions) and LC phase (light blue regions) are observable in the ternary diagrams. These results indicate that CHOL has a condensing effect in the ternary mixtures. At intermediate surface pressures (15–20 mN m^{-1}), K_s values increase in the regions rich in CHOL, especially in the low molar fraction of CCM (yellow and green regions). In monolayers at high surface pressures (30–40 mN m^{-1}), the LE phase is only observable in regions with a very high content of CCM whilst as the molar fraction of CCM decreases the phases are more condensed until they reach the LC-S transition phase (orange and red regions). At 40 mN m^{-1} the more condensed monolayers correspond to the $x_{DPPC}/x_{CHOL}/x_{CCM}$ = 0.4/0.5/0.1 (K_s = 338 mN m^{-1} at 40 mN m^{-1}) and 0.5/0.4/0.1 (K_s = 331 mN m^{-1} at 40 mN m^{-1}), while the more fluid monolayers are those with $x_{DPPC}/x_{CHOL}/x_{CCM}$ = 0.05/0.05/0.9 (K_s = 16 mN m^{-1} at 15 mN m^{-1} and K_s = 20 mN m^{-1} at 20 mN m^{-1}).

In good agreement with the observations for the A^E, the regions rich in DPPC and low in CHOL exhibit positive ΔG_m^E values for the whole range of CCM molar fractions, with particularly high ΔG_m^E values for high CCM molar fractions

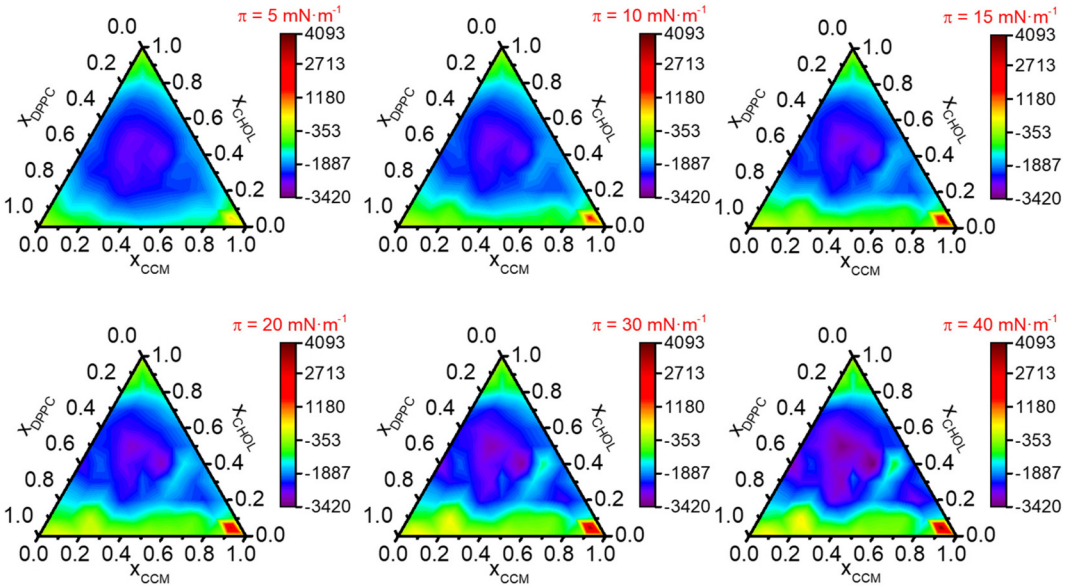

Fig. 5 ΔG_m expressed in J mol^{-1} *vs.* molar fraction in (DPPC/CHOL/CCM) ternary system for the indicated surface pressures.

(Fig. S10†). In contrast, regions with x_{CHOL} above 0.5 exhibit negative ΔG_m^E values, which is indicative of a good miscibility between the components. In the ternary mixtures (DPPC/CHOL/CCM) the Gibbs energy of mixing shows practically negative values for all molar ratios, with a few exceptions that remarkably include the regions rich in CCM and DPPC but poor in CHOL; in good agreement with the observations obtained for the binary systems, which confirms the hypothesis that CHOL acts as a key component to promote the miscibility and stability in membranes containing DPPC and CCM.

Additionally, the central region in the ternary diagram (ratios in the proximity of the $x_{DPPC}/x_{CHOL}/x_{CCM}$ = 0.33/0.33/0.33) exhibits negative ΔG_m values (Fig. 5). These results indicate that the stability of the mixed monolayers is higher than that of the pure compounds for most of the DPPC/CHOL/CCM molar fractions and in particular for the $x_{DPPC}/x_{CHOL}/x_{CCM}$ = 0.33/0.33/0.33 and close values, with the lowest ΔG_m (and consequently, higher stability of the mixed film) obtained at a surface pressure of 40 mN m^{-1} and $x_{DPPC}/x_{CHOL}/x_{CCM}$ = 0.2/0.4/0.4 (ΔG_m = −3412 J mol^{-1}) and $x_{DPPC}/x_{CHOL}/x_{CCM}$ = 0.3/0.5/0.2 (ΔG_m = −3292 J mol^{-1}). On the contrary, the less stable ternary monolayers are $x_{DPPC}/x_{CHOL}/x_{CCM}$ = 0.05/0.05/0.9 (ΔG_m = 4123 J mol^{-1} at 40 mN m^{-1}), *i.e.*, at high surface pressures and high CCM ratios.

As already mentioned, eukaryotic plasma membranes contain up to one molecule of cholesterol per every phospholipid molecule. In order to understand CCM interactions with a model that resembles the cell membrane, we analyse in detail the regions with DPPC/CHOL maintaining a x_{DPPC}/x_{CHOL} = 0.5/0.5 proportion between these two components, as indicated for clarifying purposes in Fig. S11.† In Table S.I† the thermodynamic parameters (A^E, ΔG_m^E, ΔG_m and K_s) are presented for the mixtures in which the ratio between DPPC and CHOL is maintained constant and in the 1/1 proportion, whilst variable amounts of CCM are added. Taking into account that the surface pressure equivalent to biological conditions is *ca.* 30 mN m^{-1}, the most favoured interactions between the components are present in the monolayer with $x_{DPPC}/x_{CHOL}/x_{CCM}$ = 0.4/0.4/0.2. Thus, for this molar fraction of CCM, the monolayers exhibit minimum A^E value (A^E = −0.02 nm^2 per molecule), minimum excess Gibbs energy of mixture and Gibbs energy of mixture values (ΔG_m^E = −146 J mol^{-1} and ΔG_m = −2735 J mol^{-1}) as well as maximum K_s value (K_s = 257 mN m^{-1}), which is indicative of attractive interactions between the molecules, resulting in a condensed phase. Another relevant observation from Table S.I.† is the opposite sign in thermodynamic parameters of the mixed layers at 30 mN m^{-1} for the monolayers containing CCM molar fractions in the 0.4 to 0.8 range, with the excess area values being negative while the excess Gibbs free energy values being positive. Very often the sign of A^E and ΔG_m^E is the same, but we note at this point that the excess Gibbs free energy is a complex quantity that reflects not only the energy balance between intermolecular interactions and the loss of entropy upon the compression but also the energy related to transitions (including bidimensional phase transitions,[65,79] phase segregation phenomena,[80] complex formation,[72] and also 3D interfacial transitions[73] such as aggregation and disaggregation effects[81]). Here the observation of negative excess areas for the CCM molar fractions in the 0.4 to 0.8 range and positive ΔG_m^E is tentatively interpreted in terms of CCM segregation phenomena out of the monolayer towards the formation of thicker domains, adding instability to the film, as it will be confirmed later with the AFM images.

Additionally, Brewster Angle Microscopy images of selected compositions have been included in the ESI (Fig. S12†). These

images support the main conclusions inferred from the thermodynamic studies with homogeneous monolayers at the air water interfase for the $x_{DPPC}/x_{CHOL}/x_{CCM}$ = 0.4/0.4/0.2.

In order to get additional information about the miscibility, phase segregation and homogeneity of these mixed films, AFM studies were performed on selected binary and ternary mixed films transferred at 30 mN m^{-1} onto mica substrates (upstroke process, which means that the hydrophilic part of the film is in contact with the mica and the hydrophobic part is outside). The transfer ratio values are provided in Table S.II.† Fig. 6 shows representative AFM images of the pure and mixed LB films. Both pure DPPC and CHOL monolayers form very homogeneous films onto mica. In contrast, the CCM monolayer shows regions of different height, being this height difference of (1.2 ± 0.2 nm) and the projection of the highest areas representing a *ca.* 72% of the total surface (see Fig. S13†). Taking into account that CCM at 30 mN m^{-1} is in a fluid phase with a K_s value of 80 mN m^{-1}, the observed topography is consistent with the presence of domains of CCM with different orientation on the surface. Regarding the binary mixtures, x_{DPPC}/x_{CHOL} = 0.5/0.5 mixed LB films are very homogeneous in good agreement with previous observations.[56] This result indicates miscibility of the two components at this ratio. In contrast, the x_{DPPC}/x_{CCM} = 0.5/0.5 mixed films exhibit a non-homogeneous topography with clearly visible domains with a height difference of 0.6 ± 0.1 nm, with 53% of the film surface being composed of the higher domains (Fig. S14†). This observation may suggest some kind of phase segregation. This hypothesis is supported by the difference in height between the DPPC molecule (2.4 ± 0.1, Fig. (1)) and the CCM molecule in a fully extended conformation (1.7 nm as determined from molecular models, Spartan 08V1.0.0), which results in a difference of (0.7 ± 0.1 nm), *i.e.*, similar to the observed 0.6 ± 0.1 nm value. This result is in good agreement with the poor miscibility and stability of the x_{DPPC}/x_{CCM} = 0.5/0.5 Langmuir films as described above, which may result in a large degree of phase separation. On the contrary, the x_{CHOL}/x_{CCM} = 0.5/0.5 LB film exhibits a very homogeneous surface indicative of a good miscibility between the components in this mixing ratio, which is in good agreement with the excess thermodynamic properties obtained at the air–water interface. Interestingly, the ternary $x_{DPPC}/x_{CHOL}/x_{CCM}$ = 0.4/0.4/0.2 LB films transferred at 30 mN $m^{-1}$are also very homogeneous. This result is indicative of a good miscibility between the three components at this molar ratio as well as the presence of a single and quite compact phase as corresponds with a K_s value of 257 mN m^{-1}. Other $x_{DPPC}/$

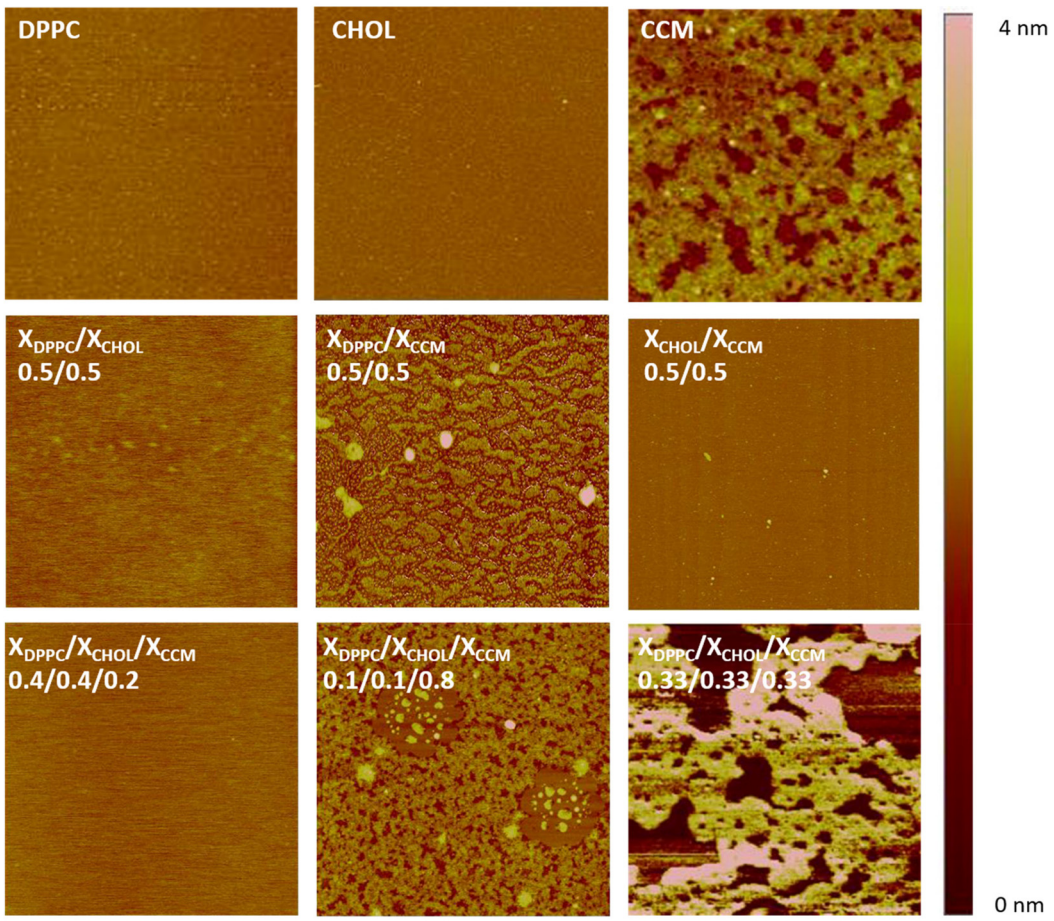

Fig. 6 2 × 2 μm²AFM images for LB films transferred at 30 mN m^{-1} for pure compounds and for mixed films at the indicated ratios.

x_{CHOL}/x_{CCM} molar ratios have been explored resulting in much less homogeneous films; for instance, $x_{DPPC}/x_{CHOL}/x_{CCM}$ = 0.1/0.1/0.8 LB films show an inhomogeneous morphology with aggregated structures (Fig. 6) or $x_{DPPC}/x_{CHOL}/x_{CCM}$ = 0.33/0.33/0.33 LB films exhibiting domains with a height difference over the mica substrate in the 3–4 nm (Fig. S15†). This is indicative of the expulsion of some molecules out of the film and either multilayer formation of these segregated regions or formation of complexes, which is consistent with the positive ΔG^{E}_{m} values obtained for this ternary mixture.

Conclusions

In this contribution, mixed binary Langmuir films of CCM with either DPPC or CHOL, as well as ternary (DPPC/CHOL/CCM) Langmuir films have been studied. At low surface pressures the addition of CCM to DPPC results in an expansion of the monolayers with respect to ideality, possibly due to rupture of hydrogen bonds in the intermolecular hydrogen bond network in CCM. At high surface pressures (>30 mN m^{-1}) such deviations become nearly negligible, which is attributed here to phase segregation, as the surface density increases. In addition, CCM induces a significant decrease in the K_s values in mixed (DPPC/CCM) monolayers in the whole range of surface pressures, *i.e.*, such monolayers are more fluid which is indicative of disruption in the ordering of the alkyl chains of DPPC. At surface pressures above 30 mN m^{-1} the values of the Gibbs energy of mixing for the (DPPC/CCM) binary system are close to zero or even positive which indicates that these monolayers are not stable. All these data together indicate that the addition of CCM to the DPPC alters the ordering and stability of the monolayer. CCM impedes lateral van der Waals interactions between the alkyl chains of neighbouring DPPC molecules, increasing the fluidity and decreasing film stability, which may also be accompanied by some phase segregation between the two components. These conclusions obtained for Langmuir films are further corroborated by the AFM studies on LB films transferred at 30 mN m^{-1}, which show that x_{DPPC}/x_{CCM} = 0.5/0.5 monolayers are non-homogeneous and point out to some phase segregation with the presence of domains whose height difference is in good agreement with the height difference between the two molecules. On the contrary, the addition of CCM to CHOL results in a condensation effect of the monolayers (except in the low CCM molar fractions, x_{CCM} < 0.2 where there is a small expansion effect). This observation together with the significant negative values obtained for the Gibbs energy of mixing indicate a good miscibility of these two compounds, which is accompanied by the presence of attractive interactions between CCM and CHOL and stable mixed monolayers with a minimum Gibbs energy of mixing at x_{CCM} = 0.6. The addition of CCM to the CHOL monolayer also results in a fluidization of the Langmuir film. The AFM images of x_{CHOL}/x_{CCM} = 0.5/0.5 mixed LB films transferred at 30 mN m^{-1} evidence the formation of a homogeneous layer on the mica substrate and therefore no evidences of phase separation.

Ternary mixtures incorporating CCM, DPPC and CHOL have also been thoroughly analysed. At low surface pressures and low CHOL molar fractions repulsive interactions between DPPC and CCM are evident. At high surface pressures (>30 mN m^{-1}) the monolayers exhibit good stability (negative Gibbs energies of mixture), particularly in the central region of the ternary diagram. CCM also induces a general fluidization of the mixed Langmuir films, which is particularly relevant in the high x_{CCM} and low x_{CHOL} regions. In general terms, the presence of CHOL in the film is mandatory to provide stability to the ternary mixture. Importantly, for mixed films in which the x_{DPPC}/x_{CHOL} = 0.5/0.5 ratio is kept constant and considering a surface pressure of 30 mN m^{-1}, *i.e.* a model that resembles the eukaryotic cell membrane, the more stable monolayers (minimum ΔG_m values) are obtained for x_{CCM} = 0.2, for which K_s also reaches a maximum value of 257 mN m^{-1} (monolayer in a solid phase). Finally, the AFM images of $x_{DPPC}/x_{CHOL}/x_{CCM}$ = 0.4/0.4/0.2 LB films indicate that highly homogenous LB monolayers are obtained for this ternary mixture. Therefore, the conclusions obtained from this study may be of interest for introducing curcumin into lipid membranes and transporting it into living cells. Further investigations of the reported $x_{DPPC}/x_{CHOL}/x_{CCM}$ = 0.4/0.4/0.2 membrane system are being carried out in our laboratories to prepare vesicles containing relevant drugs within the inner core and CCM as a co-adjuvant incorporated in the external membrane.

In addition, most studies aimed at producing novel liposomal formulations use the trial-and-error method. Therefore, a rational design of lipid formulations to develop liposomes for drug administration is of current interest, which is especially important for water-based medications that are not soluble. For these reasons, the strategy presented in this contribution – based on the thermodynamic stability and structure of the lipid mixtures – could be extended to other drugs and can contribute to diminishing the required experimentation for liposomal formulations.

Conflicts of interest

There are no conflicts to declare.

Acknowledgements

Authors acknowledge DGA/Fondos FEDER (Construyendo Europa desde Aragón) for funding the research group Platón (E31_20R) and also for financial assistance from project LMP154_21. Authors also acknowledge Dr N. Aliaga-Alcalde and A. González-Campo from the Institute of Materials Science of Barcelona (ICMAB-CSIC) for useful discussions on the CCM behavior.

References

1 D. Perrone, F. Ardito, G. Giannatempo, M. Dioguardi, G. Troiano, L. Lo Russo, A. De Lillo, L. Laino and L. Lo

Muzio, Biological and therapeutic activities, and anticancer properties of curcumin, *Exp. Ther. Med.*, 2015, **10**, 1615–1623.

2 M. E. Abd El-Hack, M. T. El-Saadony, A. A. Swelum, M. Arif, M. M. A. Ghanima, M. Shukry, A. Noreldin, A. E. Taha and K. A. El-Tarabily, Curcumin, the active substance of turmeric: its effects on health and ways to improve its bioavailability, *J. Sci. Food Agric.*, 2021, **101**, 5747–5762.

3 Y. Feng, N. Wang, F. Cheung, M. Zhu, H. Li and Y. Feng, Molecular and Cellular Mechanism Studies on Anticancer Effects of Chinese Medicines, *Biomed. Eng., Trends, Res. Technol.*, 2014, 331–362.

4 T. Farooqui and A. A. Farooqui, Curcumin: Historical Background, Chemistry, Pharmacological Action, and Potential Therapeutic Value, in *Curcumin for Neurological and Psychiatric Disorders*, Academic Press, 2019, ch. 2, pp. 23–44.

5 K. Nair, *The Agronomy and Economy of Turmeric and Ginger: the invaluable Medicinal Spice Crops*, Elsevier, Amsterdam, 2013.

6 M. Heger, Don't discount all curcumin trial data, *Nature*, 2017, **543**, 40–40.

7 H. Hatcher, R. Planalp, J. Cho, F. M. Tortia and S. V. Torti, Curcumin: From ancient medicine to current clinical trials, *Cell. Mol. Life Sci.*, 2008, **65**, 1631–1652.

8 J. Ravindran, S. Prasad and B. B. Aggarwal, Curcumin and Cancer Cells: How Many Ways Can Curry Kill Tumor Cells Selectively?, *AAPS J.*, 2009, **11**, 495–510.

9 B. B. Aggarwal and B. Sung, Pharmacological basis for the role of curcumin in chronic diseases: an age-old spice with modern targets, *Trends Pharmacol. Sci.*, 2009, **30**, 85–94.

10 A. Shehzad, F. Wahid and Y. S. Lee, Curcumin in Cancer Chemoprevention: Molecular Targets, Pharmacokinetics, Bioavailability, and Clinical Trials, *Arch. Pharm.*, 2010, **343**, 489–499.

11 H. Y. Zhou, C. S. Beevers and S. L. Huang, The Targets of Curcumin, *Curr. Drug Targets*, 2011, **12**, 332–347.

12 G. Liang, Recent progress and novel insights in curcumin research "from chemistry to clinical use", *Curr. Pharm. Des.*, 2013, **19**, 23116318.

13 S. Prasad, S. C. Gupta, A. K. Tyagi and B. B. Aggarwal, Curcumin, a component of golden spice: From bedside to bench and back, *Biotechnol. Adv.*, 2014, **32**, 1053–1064.

14 S. Prasad, A. K. Tyagi and B. B. Aggarwal, Recent Developments in Delivery, Bioavailability, Absorption and Metabolism of Curcumin: the Golden Pigment from Golden Spice, *Cancer Res. Treat.*, 2014, **46**, 2–18.

15 P. D. Kasi, R. Tamilselvam, K. Skalicka-Wozniak, S. F. Nabavi, M. Daglia, A. Bishayee, H. Pazoki-toroudi and S. M. Nabavi, Molecular targets of curcumin for cancer therapy: an updated review, *Tumor Biol.*, 2016, **37**, 13017–13028.

16 A. B. Kunnumakkara, D. Bordoloi, G. Padmavathi, J. Monisha, N. K. Roy, S. Prasad and B. B. Aggarwal, Curcumin, the golden nutraceutical: multitargeting for multiple chronic diseases, *Br. J. Pharmacol.*, 2017, **174**, 1325–1348.

17 A. Giordano and G. Tommonaro, Curcumin and Cancer, *Nutrients*, 2019, **11**, 2376.

18 D. T. Zheng, C. X. Huang, H. H. Huang, Y. Zhao, M. R. U. Khan, H. Zhao and L. J. Huang, Antibacterial Mechanism of Curcumin: A Review, *Chem. Biodivers.*, 2020, **17**, e2000171.

19 N. A. D'Angelo, M. A. Noronha, I. S. Kurnik, M. C. C. Câmara, J. M. Vieira, L. Abrunhosa, J. T. Martins, T. F. R. Alves, L. L. Tundisi, J. A. Ataide, J. S. R. Costa, A. F. Jozala, L. O. Nascimento, P. G. Mazzola, M. V. Chaud, A. A. Vicente and A. M. Lopes, Curcumin encapsulation in nanostructures for cancer therapy: A 10-year overview, *Int. J. Pharm.*, 2021, **604**, 120534.

20 A. L. Cheng, C. H. Hsu, J. K. Lin, M. M. Hsu, Y. F. Ho, T. S. Shen, J. Y. Ko, J. T. Lin, B. R. Lin, M. S. Wu, H. S. Yu, S. H. Jee, G. S. Chen, T. M. Chen, C. A. Chen, M. K. Lai, Y. S. Pu, M. H. Pan, Y. J. Wang, C. C. Tsai and C. Y. Hsieh, Phase I clinical trial of curcumin, a chemopreventive agent, in patients with high-risk or pre-malignant lesions, *Anticancer Res.*, 2001, **21**, 2895–2900.

21 W. Sun, S. Wang, W. W. Zhao, C. H. Wu, S. H. Guo, H. W. Gao, H. X. Tao, J. J. Lu, Y. T. Wang and X. P. Chen, Chemical constituents and biological research on plants in the genus Curcuma, *Crit. Rev. Food Sci. Nutr.*, 2017, **57**, 1451–1523.

22 K. M. Nelson, J. L. Dahlin, J. Bisson, J. Graham, G. F. Pauli and M. A. Walters, The Essential Medicinal Chemistry of Curcumin, *J. Med. Chem.*, 2017, **60**, 1620–1637.

23 M. Baker, Deceptive curcumin offers cautionary tale for chemists, *Nature*, 2017, **541**, 144–145.

24 A. Goel, A. B. Kunnumakkara and B. B. Aggarwal, Curcumin as "Curecumin": From kitchen to clinic, *Biochem. Pharmacol.*, 2008, **75**, 787–809.

25 M. M. Yallapu, M. Jaggi and S. C. Chauhan, Curcumin nanoformulations: a future nanomedicine for cancer, *Drug Discovery*, 2012, **17**, 71–80.

26 O. Naksuriya, S. Okonogi, R. M. Schiffelers and W. E. Hennink, Curcumin nanoformulations: A review of pharmaceutical properties and preclinical studies and clinical data related to cancer treatment, *Biomaterials*, 2014, **35**, 3365–3383.

27 S. Wanninger, V. Lorenz, A. Subhan and F. T. Edelmann, Metal complexes of curcumin – synthetic strategies, structures and medicinal applications, *Chem. Soc. Rev.*, 2015, **44**, 4986–5002.

28 A. Araiza-Calahorra, M. Akhtar and A. Sarkar, Recent advances in emulsion-based delivery approaches for curcumin: From encapsulation to bioaccessibility, *Trends Food Sci. Technol.*, 2018, **71**, 155–169.

29 M. N. Oskouie, N. S. Aghili Moghaddam, A. E. Butler, P. Zamani and A. Sahebkar, Therapeutic use of curcumin-encapsulated and curcumin-primed exosomes, *J. Cell. Physiol.*, 2019, **234**, 8182–8191.

30 Z. Rafiee, M. Nejatian, M. Daeihamed and S. M. Jafari, Application of curcumin-loaded nanocarriers for food, drug and cosmetic purposes, *Trends Food Sci. Technol.*, 2019, **88**, 445–458.

31 T. Jiang, W. Liao and C. Charcosset, Recent advances in encapsulation of curcumin in nanoemulsions: A review of encapsulation technologies, bioaccessibility and applications, *Int. Food Res. J.*, 2020, **132**, 109035.
32 C.-H. Tang, Nanocomplexation of proteins with curcumin: From interaction to nanoencapsulation (A review), *Food Hydrocolloids*, 2020, **109**, 106106.
33 D. Limón, P. Gil-Lianes, L. Rodríguez-Cid, H. L. Alvarado, N. Díaz-Garrido, M. Mallandrich, L. Baldomà, A. C. Calpena, C. Domingo, N. Aliaga-Alcalde, A. González-Campo and L. Pérez-García, Supramolecular Hydrogels Consisting of Nanofibers Increase the Bioavailability of Curcuminoids in Inflammatory Skin Diseases, *ACS Appl. Nano Mater.*, 2022, **5**, 13829–13839.
34 F. D. Feltrin, T. Agner, C. Sayer and L. M. F. Lona, Curcumin encapsulation in functional PLGA nanoparticles: A promising strategy for cancer therapies, *Adv. Colloid Interface Sci.*, 2022, **300**, 102582.
35 M. Zhang, X. L. Zhang, T. R. Tian, Q. Zhang, Y. T. Wen, J. Y. Zhu, D. X. Xiao, W. T. Cui and Y. F. Lin, Anti-inflammatory activity of curcumin-loaded tetrahedral framework nucleic acids on acute gouty arthritis, *Bioact. Mater.*, 2022, **8**, 368–380.
36 S. A. Kotenkov, O. I. Gnezdilov, A. V. Khaliullina, O. N. Antzutkin, R. S. Gimatdinov and A. V. Filippov, Effect of Cholesterol and Curcumin on Ordering of DMPC Bilayers, *Appl. Magn. Reson.*, 2019, **50**, 511–520.
37 D. F. Kucik, E. L. Elson and M. Sheetz, Weak dependence of mobility of membrane protein aggregates on aggregate size supports a viscous model of retardation of diffusion, *Biophys. J.*, 1999, **76**, 314–322.
38 S. L. Keller, Miscibility transitions and lateral compressibility in liquid phases of lipid monolayers, *Langmuir*, 2003, **19**, 1451–1456.
39 G. Brezesinski and H. Möhwald, Langmuir monolayers to study interactions at model membrane surfaces, *Adv. Colloid Interface Sci.*, 2003, **100–102**, 563–584.
40 A. Fernandez-Botello, F. Comelles, M. A. Alsina, P. Cea and F. Reig, A Monolayer Study on Interactions of Docetaxel with Model Lipid Membranes, *J. Phys. Chem. B*, 2008, **112**, 13834–13841.
41 J. V. M. Girón, R. C. Vico, B. Maggio, E. Zelaya, A. Rubert, G. Benítez, P. Carro, R. C. Salvarezza and M. E. Vela, Role of the capping agent in the interaction of hydrophilic Ag nanoparticles with DMPC as a model biomembrane, *Environ. Sci. Nano*, 2016, **3**, 462–472.
42 S. Ruiz-Rincón, A. González-Orive, V. Grazú, R. M. Fratila, J. M. d. l. Fuente and P. Cea, Altering model cell membranes by means of localized magnetic heating, *Colloids Surf., B*, 2020, **196**, 111315.
43 F. J. Pavinatto, L. Caseli, A. Pavinatto, D. S. dos Santos, T. M. Nobre, M. E. D. Zaniquelli, H. S. Silva, P. B. Miranda and O. N. de Oliveira, Probing chitosan and phospholipid interactions using Langmuir and Langmuir-Blodgett films as cell membrane models, *Langmuir*, 2007, **23**, 7666–7671.
44 A. A. Torrano, A. S. Pereira, O. N. Oliveira and A. Barros-Timmons, Probing the interaction of oppositely charged gold nanoparticles with DPPG and DPPC Langmuir monolayers as cell membrane models, *Colloids Surf., B*, 2013, **108**, 120–126.
45 T. M. Nobre, F. J. Pavinatto, L. Caseli, A. Barros-Timmons, P. Dynarowicz-Latka and O. N. Oliveira, Interactions of bioactive molecules & nanomaterials with Langmuir monolayers as cell membrane models, *Thin Solid Films*, 2015, **593**, 158–188.
46 C. G. Siontorou, G. P. Nikoleli, D. P. Nikolelis and S. K. Karapetis, Artificial Lipid Membranes: Past, Present, and Future, *Membranes*, 2017, **7**, 38.
47 O. N. Oliveira, L. Caseli and K. Ariga, The Past and the Future of Langmuir and Langmuir–Blodgett Films, *Chem. Rev.*, 2022, **122**, 6459–6513.
48 G. Xu, C. Hao, L. Zhang and R. Sun, Investigation of Surface Behavior of DPPC and Curcumin in Langmuir Monolayers at the Air-Water Interface, *Scanning*, 2017, **2017**, 6582019.
49 M. Girardon, B. Korchowiec, J. Korchowiec, E. Rogalska, N. Canilho and A. Pasc, A way to introducing a hydrophilic bioactive agent into model lipid membranes. The role of cetyl palmitate in the interaction of curcumin with 1,2-dioleoyl-sn-glycero-3-phosphatidylcholine monolayers, *J. Mol. Liq.*, 2020, **308**, 113040.
50 S. Bustin, *Molecular biology of the cell*, 2015, DOI: **10.3390/ijms161226074**.
51 P. O. Nkadi, T. A. Merritt and D.-A. M. Pillers, An overview of pulmonary surfactant in the neonate: Genetics, metabolism, and the role of surfactant in health and disease, *Mol. Genet. Metab.*, 2009, **97**, 95–101.
52 P. Toimil, G. Prieto, J. J. Miñones and F. Sarmiento, A comparative study of F-DPPC/DPPC mixed monolayers. Influence of subphase temperature on F-DPPC and DPPC monolayers, *Phys. Chem. Chem. Phys.*, 2010, **12**, 13323–13332.
53 N. Arashiki, M. Saito, I. Koshino, K. Kamata, J. Hale, N. Mohandas, S. Manno and Y. Takakuwa, An unrecognized function of cholesterol: regulating the mechanism controlling membrane phospholipid asymmetry, *Biochemistry*, 2016, **55**, 3504–3513.
54 D. Marsh, Lateral pressure in membranes, *Biochim. Biophys. Acta, Biomembr.*, 1996, **1286**, 183–223.
55 G. Cevc and D. Marsh, *Phospholipid Bilayers. Physical Principles and Models*, Wiley-Interscience, New York, 1987.
56 S. Ruiz-Rincon, A. Gonzalez-Orive, J. M. de la Fuente and P. Cea, Reversible Monolayer-Bilayer Transition in Supported Phospholipid LB Films under the Presence of Water: Morphological and Nanomechanical Behavior, *Langmuir*, 2017, **33**, 7538–7547.
57 D. Marsh, Lateral pressure in membranes, *Biochim. Biophys. Acta, Biomembr.*, 1996, **1283**, 183–223.
58 J. T. Davies and E. K. Rideal, *Interfacial Phenomena*, Academic Press, New York, 1963.
59 P. Mattjus, R. Bittman and J. P. Slotte, Molecular Interaction and Lateral Domain Formation in Monolayers

Containing Cholesterol and Phosphatidylcholines with Acyl- or Alkyl-Linked C16 Chains, *Langmuir*, 1996, **12**, 1284–1290.

60 R. Seoane, J. Miñones, O. Conde, M. Casas and E. Iribarnegaray, Thermodynamic and Brewster Angle Microscopy Studies of Fatty Acid/Cholesterol Mixtures at the Air/Water Interface, *J. Phys. Chem. B*, 2000, **104**, 7735–7744.

61 E. E. Berring, K. Borrenpohl, S. J. Fliesler and A. B. Serfis, A comparison of the behavior of cholesterol and selected derivatives in mixed sterol–phospholipid Langmuir monolayers: a fluorescence microscopy study, *Chem. Phys. Lipids*, 2005, **136**, 1–12.

62 J.-C. Wu, T.-L. Lin, C.-P. Yang, U. S. Jeng, H.-Y. Lee and M.-C. Shih, X-ray reflectivity and BAM studies on the LB film of mixed DPPC/DC-cholesterol monolayer, *Colloids Surf., A*, 2006, **284–285**, 103–108.

63 K. Sabatini, J.-P. Mattila and P. K. J. Kinnunen, Interfacial Behavior of Cholesterol, Ergosterol, and Lanosterol in Mixtures with DPPC and DMPC, *Biophys. J.*, 2008, **95**, 2340–2355.

64 K. B. Lintker, P. Kpere-Daibo, S. J. Fliesler and A. B. Serfis, A comparison of the packing behavior of egg phosphatidylcholine with cholesterol and biogenically related sterols in Langmuir monolayer films, *Chem. Phys. Lipids*, 2009, **161**, 22–31.

65 M. Jurak, Thermodynamic Aspects of Cholesterol Effect on Properties of Phospholipid Monolayers: Langmuir and Langmir-Blodgett Monolayer Study, *J. Phys. Chem. B*, 2013, **117**, 3496–3502.

66 R. P. Giri, A. Chakrabarti and M. K. Mukhopadhyay, Cholesterol-Induced Structural Changes in Saturated Phospholipid Model Membranes Revealed through X-ray Scattering Technique, *J. Phys. Chem. B*, 2017, **121**, 4081–4090.

67 Y. Manolova, V. V. Deneva, L. Antonov, E. Drakalska, D. B. Momekova and N. Lambov, The effect of the water on the curcumin tautomerism: a quantitative approach, *Spectrochim. Acta, Part A*, 2014, **132**, 815–820.

68 A. Karewicz, D. Bielska, B. Gzyl-Malcher, M. Kepczynski, R. Lach and M. Nowakowska, Interaction of curcumin with lipid monolayers and liposomal bilayers, *Colloids Surf., B*, 2011, **88**, 231–239.

69 D. J. Crisp, Surface Chemistry Suppl. Research (London), in *Surface Chemistry Suppl. Research (London)*, 1949, pp. 17–23.

70 A. W. Adamson and A. P. Gast, *Physical Chemistry of Surfaces*, John Wiley & Sons, New York, 6th edn, 1997.

71 D. A. Cadenhead and F. Müller-Landau, Molecular accommodation and molecular interactions in mixed insoluble monomolecular films, *J. Colloid Interface Sci.*, 1980, **78**, 269–270.

72 M. Haro, B. Giner, C. Lafuente, M. C. Lopez, F. M. Royo and P. Cea, Proton sponge and fatty acid interactions at the air-water interface. Thermodynamic, spectroscopic, and microscopic study, *Langmuir*, 2005, **21**, 2796–2803.

73 M. Mottola, B. Caruso and M. A. Perillo, Langmuir films at the oil/water interface revisited, *Sci. Rep.*, 2019, **9**, 2259.

74 F. C. Goodrich, *Proceedings of the Second International Congress of Surface Activity*, 1956, vol. I, p. 85.

75 R. E. Pagano and N. L. Gershfeld, Physical chemistry of lipid films at the air-water interface. II. Binary lipid mixtures. Principles governing miscibility of lipids in surfaces, *J. Phys. Chem.*, 1972, **76**, 1238–1243.

76 P. Dynarowicz-Łątka and K. Kita, Molecular interaction in mixed monolayers at the air/water interface, *Adv. Colloid Interface Sci.*, 1999, **79**, 1–17.

77 M. Haro, P. Cea, I. Gascón, F. M. Royo and M. C. López, Mixed Langmuir and Langmuir–Blodgett films of a proton sponge and a fatty acid: influence of the subphase nature on the interactions between the two components, *J. Phys. Chem. B*, 2007, **111**, 2845.

78 A. V. Filippov, S. A. Kotenkov, B. V. Munavirov, A. V. Khaliullina, O. I. Gnezdilov and O. N. Antzutkin, Effect of curcumin on lateral diffusion in lipid bilayers, *Mendeleev Commun.*, 2016, **26**, 109–110.

79 M. Jurak, K. Szafran, P. Cea and S. Martín, Analysis of Molecular Interactions between Components in Phospholipid-Immunosuppressant-Antioxidant Mixed Langmuir Films, *Langmuir*, 2021, **37**, 5601–5616.

80 A. Villares, S. Martin, I. Giner, J. Diaz, D. P. Lydon, P. J. Low and P. Cea, The use of scanning polarization force microscopy to study the miscibility of a molecular wire candidate and an insulating fatty acid in mixed LB films, *Soft Matter*, 2008, **4**, 1508–1514.

81 G. A. Georgiev, E. Kutsarova, A. Jordanova, R. Krastev and Z. Lalchev, Interactions of Meibomian gland secretion with polar lipids in Langmuir monolayers, *Colloids Surf., B*, 2010, **78**, 317–327.